Electromagnetic tunneling of obliquely incident waves through a single-negative slab paired with a double-positive uniaxial slab

Giuseppe Castaldi,[1] Vincenzo Galdi,[1,*] Andrea Alù,[2] and Nader Engheta[3]

[1]*CNR-SPIN and Waves Group, Department of Engineering, University of Sannio, I-82100, Benevento, Italy*
[2]*Department of Electrical and Computer Engineering, The University of Texas at Austin, Austin, Texas 78712, USA*
[3]*Department of Electrical and Systems Engineering, University of Pennsylvania, Philadelphia, Pennsylvania 19104, USA*
**Corresponding author: vgaldi@unisannio.it*

Received June 17, 2011; accepted July 24, 2011;
posted July 29, 2011 (Doc. ID 149448); published September 6, 2011

We show that, under appropriate oblique-incidence and polarization conditions, the inherent opaqueness of a homogeneous, isotropic single-negative slab may be perfectly compensated (in the ideal lossless case) by a homogeneous, anisotropic (uniaxial) double-positive slab, so that complete tunneling (with total transmission and zero phase delay) occurs. We present an analytical and numerical study aimed at deriving the basic design rules, elucidating the underlying physical mechanisms, and exploring the role of the various involved parameters. © 2011 Optical Society of America

OCIS codes: 260.5740, 240.7040, 160.3918.

1. INTRODUCTION AND BACKGROUND

Single-negative (SNG) materials, characterized by only one negative (real part) constitutive parameter, are essentially opaque to electromagnetic (EM) radiation, in view of the dominant imaginary character of the propagation constant, even in the ideal lossless case. However, they can give rise to very intriguing, and somehow counterintuitive, field effects when inserted in heterostructures under proper matching conditions. For instance, Fredkin and Ron [1] observed that a layered material composed of alternating epsilon-negative (ENG) and mu-negative (MNG) layers, in spite of the inherent opaqueness of its constituents, was capable of supporting propagating modes, effectively exhibiting either a negative- (see also [2]) or positive-refractive-index character. Alù and Engheta [3] focused instead on homogeneous, isotropic ENG-MNG bilayers, and they showed that resonant tunneling phenomena (with total transmission and zero phase-delay) might occur under suitable matching conditions. Some of their results may also be interpreted in the more general framework of complementary media introduced by Pendry and Ramakrishna [4], which also allows straightforward extension to anisotropic, inhomogeneous configurations.

Building on the above results, further extensions and generalizations have been proposed in [5–21], including one-dimensional photonic crystals [5,6,9,10,12], noncontiguous layers [15], "nonconjugated" pairs [17], transformation-optics-inspired configurations [19], as well as general heterostructures containing impedance-mismatched metamaterial layers [13], and, more specifically, SNG layers paired with double-negative (i.e., negative permittivity and permeability) [11,14] or double-positive (i.e., positive permittivity and permeability—DPS) [7,8,16,18,20,21] layers.

Especially relevant for the present investigation are the SNG-DPS configurations in [7,8,16,18,20,21]. While it can readily be proved analytically [7] that, for normal incidence, a single (homogeneous, isotropic) DPS slab cannot perfectly compensate the opaqueness of an SNG slab, it was shown in [7,8,18,21] that complete tunneling may actually occur through an ENG layer symmetrically sandwiched between high-permittivity DPS layers (see also the related theoretical and numerical study in [22]). Such results were also demonstrated experimentally at microwave frequencies by synthesizing the required metamaterials via resonant (H-shaped, mesh, split-ring) metallic inclusions [7,8,18]. In [20], we extended the above results to asymmetrical trilayers composed of an ENG slab paired (at one side only) with a bilayer of homogeneous DPS materials. For an assigned frequency and normally incident illumination, we derived analytically the design rules for such a DPS bilayer to compensate the opaqueness of a given ENG slab. Moreover, we showed that, under the above conditions, the DPS bilayer would effectively mimic (in terms of wave impedance and reflection properties) an equivalent "matched" (according to [3]) MNG slab, over a moderately wide (~10%) bandwidth. Considering the relative challenge in realizing magnetic metamaterials with negative permeability, particularly at higher frequencies, it is remarkable that a proper combination of DPS slabs may effectively act as an MNG layer.

Interestingly, it was shown in [16] that zero reflection may actually occur for an ENG-DPS bilayer, under obliquely incident transverse magnetic (TM) polarized illumination. However, the study in [16] was limited to the bare mathematical derivation of the reflectionless condition. In this paper, we study in detail the hitherto unexplored physical mechanisms underlying this very intriguing phenomenon and their possible implications. In this framework, we consider a more general configuration featuring a homogeneous, isotropic SNG slab paired with a uniaxially anisotropic DPS slab, which provides an additional tuning parameter. Unlike the Fabry–Perot-type resonant phenomena observed in [7,8,18,20,21] (characterized

 © 2011 Optical Society of America

by standing waves in the DPS layers and a nonzero phase delay), the resonant phenomena in the proposed configuration are mediated by the excitation of localized surface modes at the SNG-DPS interface, are characterized by zero phase delay, and they depend on the slab thickness ratio (rather than sum), in a much closer analogy with what observed in the matched ENG-MNG bilayers [3]. This allows us to establish a more direct and physically incisive analogy between the uniaxial-DPS slab and a matched (homogeneous, isotropic) SNG slab, which may turn out useful to simplify the realization of some equivalent magnetic effects at high frequencies.

Accordingly, the rest of the paper is laid out as follows. In Section 2, we outline the problem geometry and formulation. In Section 3, we derive the main analytical results, starting with the resonant tunneling conditions and proceeding with the analogy between the uniaxial-DPS slab and a matched SNG slab. In Section 4, we present and discuss some representative numerical examples, and we investigate the sensitivity of the tunneling phenomena to frequency, polarization, and incidence direction of the illumination, as well as the effects of the unavoidable material dispersion and losses. Some brief concluding remarks follow in Section 5.

2. PROBLEM GEOMETRY AND STATEMENT

Without loss of generality, the two-dimensional configuration under study, illustrated in the Cartesian (x, y, z) reference coordinate system of Fig. 1, comprises a homogeneous, isotropic ENG slab of thickness d_1 and relative permittivity ε_1 (with $\mathrm{Re}(\varepsilon_1) < 0$), paired with a homogeneous, generally anisotropic (uniaxial) DPS slab of thickness d_2 and relative permittivity tensor

$$\underline{\underline{\varepsilon_2}} = \begin{bmatrix} \varepsilon_{2\perp} & 0 & 0 \\ 0 & \varepsilon_{2\parallel} & 0 \\ 0 & 0 & \varepsilon_{2\parallel} \end{bmatrix}, \qquad \mathrm{Re}(\varepsilon_{2\perp}) > 0, \qquad \mathrm{Re}(\varepsilon_{2\parallel}) > 0. \tag{1}$$

Both slabs are assumed as nonmagnetic (i.e., $\mu_1 = \mu_2 = 1$), infinitely long in the y and z directions, and immersed in vacuum. We assume time-harmonic ($\exp(-i\omega t)$), unit-amplitude, obliquely incident (with angle θ_i; see Figure 1), TM-polarized plane-wave illumination, with a z-directed magnetic field

$$H_z^i(x, y) = \exp[ik(x\cos\theta_i + y\sin\theta_i)], \tag{2}$$

where $k = \omega/c = 2\pi/\lambda$ denotes the vacuum wavenumber and c and λ are the corresponding speed of light and wavelength, respectively. In what follows, we outline the general analytical solution of the problem, and derive the conditions for total transmission.

3. ANALYTICAL DERIVATIONS

A. Generalities

In the ideal lossless case, the magnetic field expression can be written as

$$H_z(x, y) = \begin{cases} H_z^i + B_0 \exp[ik(-x\cos\theta_i + y\sin\theta_i)], & x < -d_1, \\ \exp(iky\sin\theta_i)[A_1\cosh(\alpha_1 x) + B_1\sinh(\alpha_1 x)], & -d_1 < x < 0, \\ \exp(iky\sin\theta_i)[A_2\cosh(\alpha_2 x) + B_2\sinh(\alpha_2 x)], & 0 < x < d_2, \\ A_3\exp[ik(x\cos\theta_i + y\sin\theta_i)], & x > d_2, \end{cases} \tag{3}$$

where the phase-matching conditions (conservation of the transverse wavenumber) at the interfaces $x = -d_1$, 0, d_2, and the radiation condition are already enforced, and

$$\alpha_1 = k\sqrt{|\varepsilon_1| + \sin^2\theta_i}, \tag{4}$$

$$\alpha_2 = k\sqrt{\varepsilon_{2\parallel}\left(\frac{\sin^2\theta_i}{\varepsilon_{2\perp}} - 1\right)}, \qquad \sin^2\theta_i > \varepsilon_{2\perp}, \tag{5}$$

denote the (real, positive) attenuation constants in the ENG and uniaxial-DPS slabs, respectively. The inequality in Eq. (5)

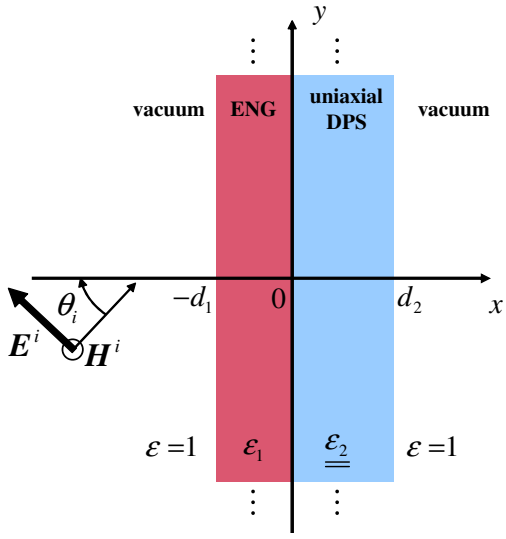

Fig. 1. (Color online) Problem schematic in the associated Cartesian reference system: we consider a homogeneous, isotropic slab of ENG material of thickness d_1 and relative permittivity ε_1 [with $\mathrm{Re}(\varepsilon_1) < 0$] paired with a homogeneous, anisotropic (uniaxial) DPS slab of thickness d_2 and relative permittivity tensor $\underline{\underline{\varepsilon_2}}$ given in Eq. (1). The bilayer is immersed in vacuum, and it is illuminated by an obliquely incident, TM-polarized plane wave.

ensures that the uniaxial-DPS slab operates below cutoff, which is instrumental in the following developments. The six unknown expansion coefficients B_0, A_1, B_1, A_2, B_2, A_3 in Eq. (3) may be computed by enforcing the tangential-field continuity at the interfaces $x = -d_1$, 0, d_2, with the electric field following from Eq. (3) and the relevant Maxwell's curl equation.

B. Conditions for Total Transmission

The analytical expressions of the expansion coefficients in Eq. (3) are not reported here for brevity. Instead, we focus on the coefficient B_0, which plays the role of the reflection coefficient. Accordingly, the total-transmission resonant condition is derived by zeroing its numerator (provided the denominator is nonzero), namely,

$$\begin{aligned}&\varepsilon_{2\|}\alpha_2(\alpha_1^2+\varepsilon_1^2k^2\cos^2\theta_i)\tanh(\alpha_1 d_1)\\&+\varepsilon_1\alpha_1(\alpha_2^2+\varepsilon_{2\|}^2k^2\cos^2\theta_i)\tanh(\alpha_2 d_2)\\&+ik\cos\theta_i(\varepsilon_1^2\alpha_2^2-\varepsilon_{2\|}^2\alpha_1^2)\tanh(\alpha_1 d_1)\tanh(\alpha_2 d_2)\\&=0.\end{aligned}\tag{6}$$

Zeroing the imaginary part of Eq. (6), and recalling Eqs. (4) and (5), we obtain

$$\varepsilon_{2\perp}=\frac{\varepsilon_1^2\sin^2\theta_i}{\varepsilon_{2\|}(|\varepsilon_1|+\sin^2\theta_i)+\varepsilon_1^2},\tag{7}$$

which automatically satisfies the inequality (cutoff condition) in Eq. (5). Substituting Eq. (7) in Eq. (6), and zeroing the remaining real part yields the second condition:

$$\frac{\varepsilon_{2\|}^2\alpha_1(\alpha_1^2+\varepsilon_1^2k^2\cos^2\theta_i)}{|\varepsilon_1|\cosh\left(\frac{\alpha_1 d_1}{\varepsilon_1}\right)\cosh\left(\frac{\varepsilon_{2\|}\alpha_1 d_1 d_2}{\varepsilon_1}\right)}\sinh\left[\alpha_1\left(d_1-d_2\frac{\varepsilon_{2\|}}{|\varepsilon_1|}\right)\right]=0,\tag{8}$$

whose general solution is

$$|\varepsilon_1|d_1=\varepsilon_{2\|}d_2.\tag{9}$$

Thus, for a given ENG slab with parameters ε_1, d_1, and for a given incidence angle θ_i, the conditions in Eqs. (7) and (9) yield an infinity of possible solutions [23] for total transmission, in terms of the three remaining parameters $\varepsilon_{2\perp}$, $\varepsilon_{2\|}$, d_1/d_2. For the case of the isotropic DPS slab ($\varepsilon_{2\perp}=\varepsilon_{2\|}$), Eqs. (7) and (9) reduce to the results in [16].

Note that the seemingly possible (trivial) solutions of Eq. (8) featuring $\varepsilon_{2\|}=0$ or $\alpha_1=0$ are inconsistent with the previous assumptions used to derive Eq. (8). Moreover, from Eq. (7), it is readily understood that, approaching normal incidence (i.e., $\theta_i\to 0$), extreme parameter values (i.e., $\varepsilon_{2\perp}\to 0$) are required in order to achieve complete tunneling.

A few other general considerations are in order. First, the total-transmission conditions in Eqs. (7) and (9) do not depend explicitly on the frequency, although an implicit frequency dependence is unavoidable in view of the inherent material dispersion in ENG materials. Also, they do not depend on the bilayer total thickness, but rather on the ratio d_1/d_2, thereby implying that the layers may be made, in principle, arbitrarily thin. The additional permittivity parameter available in our anisotropic configuration allows more flexibility in the choice of d_1/d_2, which is instead bounded for the isotropic case [16]. This may be particularly useful for strongly opaque ENG layers (i.e., $|\varepsilon_1|\gg 1$) and nearly normal incidence. Next, it can be shown that, under total-transmission conditions, the expansion coefficient A_3 in Eq. (3) reduces to

$$A_3=\exp[-ik\cos\theta_i(d_1+d_2)],\tag{10}$$

so that the total phase-delay accumulated through the bilayer is zero. Moreover, looking at the expression of the field intensity in the bilayer under total-transmission conditions,

$$|H_z(x)|^2=\begin{cases}\left\{\cosh^2[\alpha_1(x+d_1)]+\frac{\varepsilon_1^2k^2\cos^2\theta_i}{\alpha_1^2}\sinh^2[\alpha_1(x+d_1)]\right\}, & -d_1<x<0,\\ \left\{\cosh^2\left[\frac{\alpha_1\varepsilon_{2\|}(x-d_2)}{\varepsilon_1}\right]+\frac{\varepsilon_1^2k^2\cos^2\theta_i}{\alpha_1^2}\sinh^2\left[\frac{\alpha_1\varepsilon_{2\|}(x-d_2)}{\varepsilon_1}\right]\right\}, & 0<x<d_2,\end{cases}\tag{11}$$

we observe that it reaches its minima at the interfaces with vacuum $x=-d_1$, $x=d_2$, and it is exponentially peaked at the ENG-DPS interface $x=0$, thereby yielding a localized surface mode.

The above features, markedly different from those exhibited by the SNG-DPS configurations considered in [7,8,18,20,21], closely resemble what was observed in connection with matched ENG-MNG bilayers studied in [3]. This suggests that the uniaxial-DPS slab in our configuration may effectively mimic an MNG slab. Below, we explore to what extent this equivalence is fulfilled.

C. Analogy between Uniaxial-DPS and MNG Media

For the assigned ENG slab parameters ε_1 and d_1, straightforward enforcement of the matching conditions in [3] yields the constitutive parameters

$$\begin{cases}\varepsilon_{2e}=\frac{d_1}{d_2}|\varepsilon_1|,\\ \mu_{2e}=\left(\frac{1}{\varepsilon_{2e}}-\frac{\varepsilon_{2e}}{\varepsilon_1^2}\right)\sin^2\theta_i-\frac{\varepsilon_{2e}}{|\varepsilon_1|},\end{cases}\tag{12}$$

of an effective homogeneous, isotropic slab of thickness d_2 that would perfectly compensate the ENG slab for the incidence angle θ_i. The medium described by the constitutive parameters in Eq. (12) is MNG for any incidence direction if $\varepsilon_{2e} \geq |\varepsilon_1|$ (i.e., $d_1 \geq d_2$). For $\varepsilon_{2e} < |\varepsilon_1|$ (i.e., $d_1 < d_2$), the MNG character is restricted to the incidence cone

$$|\sin\theta_i| \leq \varepsilon_{2e}\sqrt{\frac{|\varepsilon_1|}{\varepsilon_1^2 - \varepsilon_{2e}^2}}. \tag{13}$$

For such an effective medium, let us consider the attenuation constant

$$\alpha_{2e} = k\sqrt{\sin^2\theta_i - \varepsilon_{2e}\mu_{2e}}, \tag{14}$$

and the transverse wave impedance

$$\eta_{2e} = \frac{i\eta\alpha_{2e}}{k\varepsilon_{2e}}, \tag{15}$$

with η denoting the vacuum characteristic impedance, and compare them with the corresponding expressions for the uniaxial-DPS medium, i.e., α_2 in Eq. (5) and

$$\eta_2 = \frac{i\eta\alpha_2}{k\varepsilon_{2\|}}. \tag{16}$$

It can readily be verified that the total-transmission conditions in Eqs. (7) and (9) yield

$$\begin{cases} \varepsilon_{2\|} = \varepsilon_{2e}, \\ \alpha_2 = \alpha_{2e}, \\ \eta_2 = \eta_{2e}. \end{cases} \tag{17}$$

In other words, the uniaxial-DPS slab exhibits the same transverse-field distributions (and, hence, reflection and transmission responses) as the matched effective slab in Eq. (12), which may be MNG under appropriate conditions [see the discussion after Eq. (12)].

The above analogy closely resembles the one exploited in [24,25] in order to emulate an MNG medium via a metallic waveguide operating below cutoff under TM polarization. Both mechanisms rely on the capacitive character of transverse wave impedance of TM-polarized evanescent fields. While, in [24,25], the underlying cutoff condition is generated by the metallic walls, in our configuration it is instead created by the material properties of a DPS uniaxial medium. This is in some ways consistent with the channeling properties of uniaxial metamaterials characterized by extreme material parameters [26]. Also in this case, strong spatial dispersion effects are hinted at by the dependence of the effective permeability [Eq. (12)] on the incidence angle. Clearly, in view of this explicit dependence on the incidence angle, and the implicit dependence on frequency (given the inherently dispersive character of SNG media), we expect the above analogy to be practically realizable only under narrow-angle/frequency conditions (see below for numerical examples).

4. REPRESENTATIVE NUMERICAL RESULTS

In order to elucidate the basic underlying phenomenology, we begin considering an ideal lossless configuration featuring a mildly opaque ENG slab with $\varepsilon_1 = -3$ and $d_1 = 0.1\lambda_0$ and an incidence direction $\theta_{i0} = 30°$; here and henceforth, the subscript "0" is used to identify the fiducial frequency/wavelength and incidence angle for which the tunneling conditions are strictly fulfilled. Among the infinite solutions of the total-transmission conditions in Eqs. (7) and (9), we select the one with $d_2 = d_1$, which yields $\varepsilon_{2\perp} = 0.12$ and $\varepsilon_{2\|} = 3$. Figure 2 shows the transverse-field (intensity and phase) distributions at resonance, from which the complete tunneling effect is clearly visible. As anticipated in Subsection 3.B, it can be observed that the effect is mediated by the excitation of a localized surface mode at the ENG-DPS interface (with evanescent field amplification in the ENG layer), and it does not imply any phase-delay accumulation. In other words, for the given polarization and incidence direction, the incident wavefront at the input interface $x = -d_1$ is perfectly reproduced at the output interface $x = d_2$, so that the bilayer effectively behaves as an EM "nullity."

It is interesting to explore the sensitivity of the phenomenon with respect to the frequency, polarization, and incidence direction of the illumination, as well as to the unavoidable material dispersion and losses. To this aim, for the same configuration above, we consider a more realistic (dispersive, lossy) Drude-type model for the ENG medium:

$$\varepsilon_1(\omega) = 1 - \frac{\omega_{p1}^2}{\omega(\omega + i\gamma_1)}, \tag{18}$$

with the plasma angular frequency ω_{p1} and the damping coefficient γ_1 adjusted so that $\mathrm{Re}[\varepsilon_1(\omega_0)] \approx -3$ (with a loss-tangent $\sim 10^{-2}$ at resonance). For the uniaxial-DPS slab, we assume a conventional mixing formula [27]:

$$\begin{cases} \varepsilon_{2\perp}(\omega) = \left[\frac{\tau}{\varepsilon_a(\omega)} + \frac{1-\tau}{\varepsilon_b}\right]^{-1}, \\ \varepsilon_{2\|}(\omega) = \tau\varepsilon_a(\omega) + (1-\tau)\varepsilon_b, \end{cases} \tag{19}$$

typical of homogenized two-phase multilayer metamaterials, with the constituents modeled as

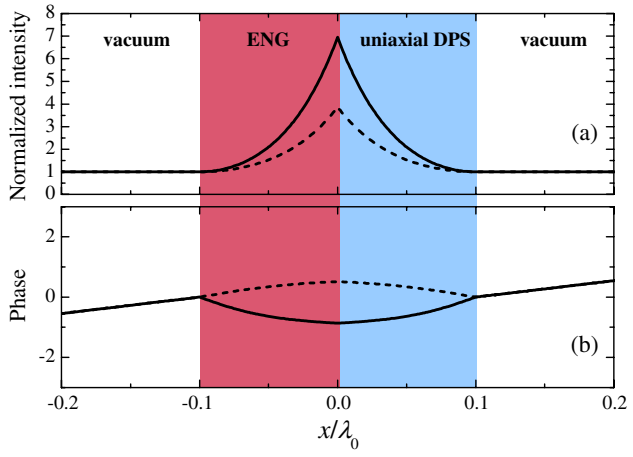

Fig. 2. (Color online) (a) Intensity and (b) phase distributions of TM (solid) and TE (dashed) fields (normalized by the incident values) at resonance, for an ideal, lossless bilayer as in Fig. 1, with $\varepsilon_1 = -3$, $d_1 = d_2 = 0.1\lambda_0$, $\varepsilon_{2\perp} = 0.12$, and $\varepsilon_{2\|} = 3$, under TM-polarized, obliquely incident illumination with $\theta_i = \theta_{i0} = 30°$.

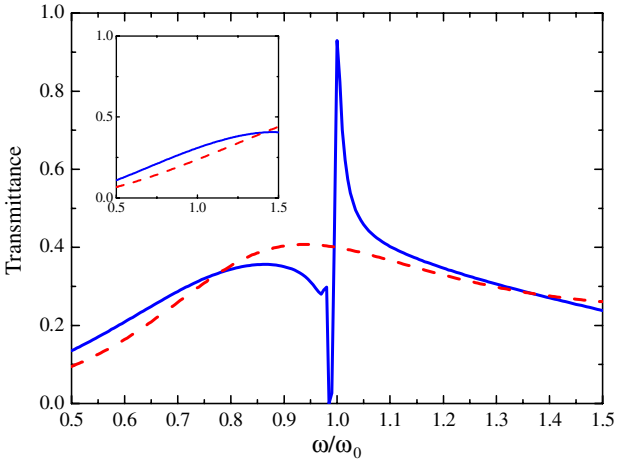

Fig. 3. (Color online) Transmittance (for $\theta_i = \theta_{i0} = 30°$) frequency response, for TM (solid blue curve) and TE (dashed red curve), pertaining to the parameter configuration as in Fig. 2, but considering for the ENG medium the Drude-type model [Eq. (18)] in with $\omega_{p1} = 2\omega_0$, $\gamma_1 = 3.75 \cdot 10^{-3}\omega_{p1}$ (so that $\mathrm{Re}[\varepsilon_1(\omega_0)] \approx -3$), and for the uniaxial-DPS medium the mixing rules in Eqs. (19) and (20), with $\tau = 0.252$, $\omega_{pa} = 0.984\omega_0$, $\gamma_a = 3.24 \cdot 10^{-4}\omega_{pa}$ (so that $\mathrm{Re}[\varepsilon_{2\perp}(\omega_0)] \approx 0.12$ and $\mathrm{Re}[\varepsilon_{2\parallel}(\omega_0)] \approx 3$). Also shown as a reference (in the inset) is the response of the stand-alone ENG slab.

$$\varepsilon_a(\omega) = 1 - \frac{\omega_{pa}^2}{\omega(\omega + i\gamma_a)}, \qquad \varepsilon_b = 4(1 + 10^{-3}i), \tag{20}$$

where the filling fraction τ and the other parameters are chosen so that $\mathrm{Re}[\varepsilon_{2\perp}(\omega_0)] \approx 0.12$ and $\mathrm{Re}[\varepsilon_{2\parallel}(\omega_0)] \approx 3$ (with a loss tangent $\sim 10^{-2}$ at resonance). Figure 3 shows the corresponding transmittance response, for both TM and TE polarizations, as a function of frequency, from which a sharp, asymmetrical resonant line shape is observed at the nominal resonant frequency for the TM polarization, with a high-transmittance peak of ~93%, i.e., nearly a threefold enhancement with respect to the typical transmittance level of the stand-alone ENG slab (also shown, as a reference, in the inset). The close-by zero-transmittance dip is attributable to a passage through zero of (the real part of) $\varepsilon_{2\perp}(\omega)$, for which the electric field at the slab entrance is required to be purely tangential, producing total reflection analogous to a perfect magnetic conductor for TM incidence [28]. Away from the resonance, as well as for the TE polarization (which does not exhibit any resonance), the transmittance levels are comparable with those typical of the stand-alone ENG slab. For the same configuration, Fig. 4 shows the angular response, from which a moderately broad transmittance peak centered at the fiducial incidence angle $\theta_i = \theta_{i0}$ is observed for the TM polarization. For an increasing level of losses, a progressive decrease in the transmittance peak amplitude is observed (not shown here for brevity), qualitatively similar to what is observed in other resonant tunneling phenomena [3].

In light of the analogy established in Subsection 3.C, it is insightful to compare the response of the uniaxial-DPS slab above with that of an effective "matched" (according to [3]) homogeneous, isotropic MNG slab of the same thickness featuring

$$\varepsilon_{2e} = 3, \qquad \mu_{2e}(\omega_0) = -1, \tag{21}$$

where we assume a Drude-type frequency dispersion for the permeability, analogous to Eq. (20). Substituting, in the

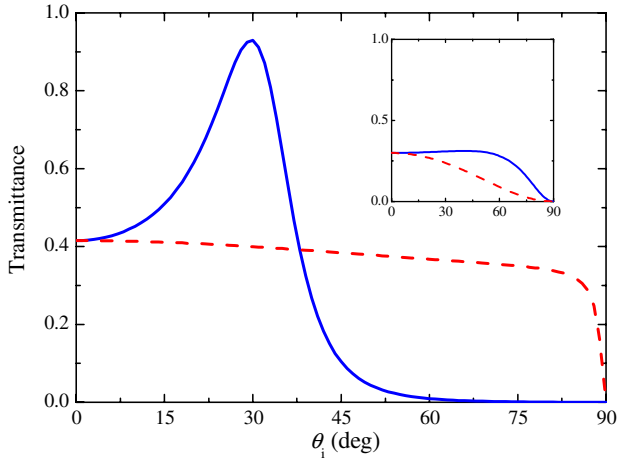

Fig. 4. (Color online) As in Fig. 3, but with an angular response at resonance.

bilayer, the uniaxial-DPS slab with such an MNG slab would yield, at the fiducial frequency and incidence angle, the same tunneling condition, with field distributions identical to those in Fig. 3. Figures 5 and 6 compare the reflection-coefficient (magnitude and phase) responses of the stand-alone (uniaxial-DPS and MNG) slabs, as a function of frequency and angle, respectively. Besides the expected perfect match of the responses at the fiducial frequency and incidence angle, it can be observed that the agreement rapidly deteriorates within a relatively small neighborhood. Qualitatively similar results (not shown here for brevity) are observed for the transmission coefficient. Therefore, we may conclude that the uniaxial-DPS slab may effectively mimic an MNG-type response only within narrow frequency/angular ranges.

As a further example, we consider a more critical configuration, featuring an ENG slab with increased opacity ($\mathrm{Re}[\varepsilon_1(\omega_0)] = -100$ and $d_1 = \lambda_0/100$) and a closer-to-normal nominal incidence direction $\theta_{i0} = 15°$. From the total-transmission conditions in Eqs. (7) and (9), selecting $d_2 = 100d_1/3 = \lambda_0/3$, we obtain $\mathrm{Re}[\varepsilon_{2\perp}(\omega_0)] = 0.065$ and

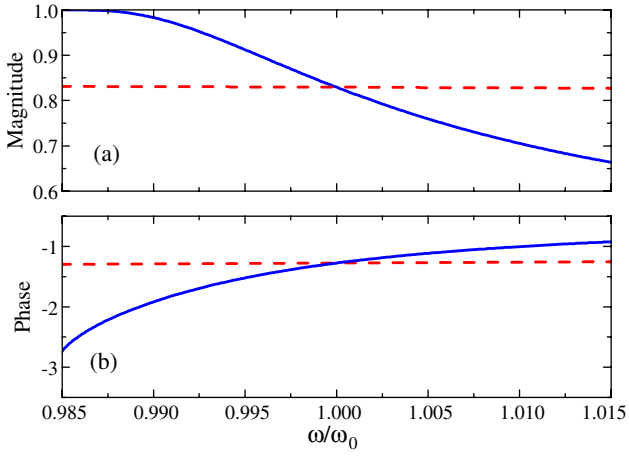

Fig. 5. (Color online) (a) Magnitude and (b) phase of the reflection-coefficient frequency response (for $\theta_i = \theta_{i0} = 30°$) pertaining to the stand-alone uniaxial-DPS slab (solid blue curve) with parameters as in Figs. 2 and 3 (for TM polarization, and assuming zero losses), compared with that of an effective (homogeneous, isotropic) matched [see Eq. (21)] MNG slab (dashed red curve), with the relative permeability described by a lossless Drude-type model $\mu_{2e}(\omega) = 1 - 2\omega_0^2/\omega^2$.

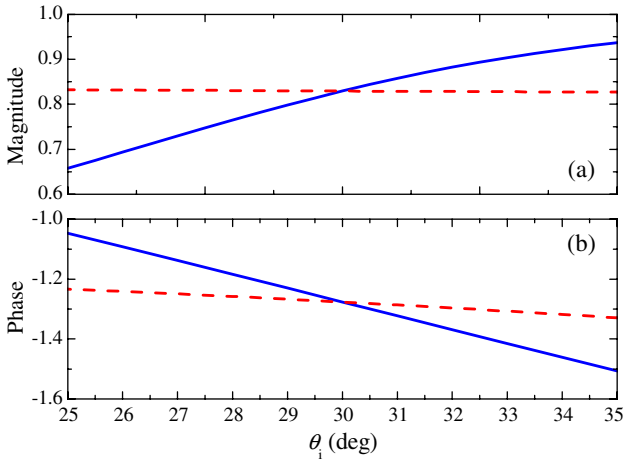

Fig. 6. (Color online) As in Fig. 5, but with an angular response at resonance.

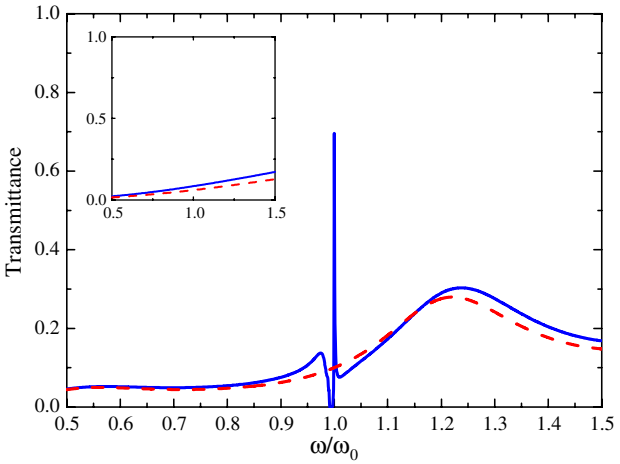

Fig. 7. (Color online) As in Fig. 3, but for $\theta_i = \theta_{i0} = 15°$, and an ENG slab [see Eq. (18)] with $\omega_{p1} = 10.05\omega_0$, $\gamma_1 = 9.85 \cdot 10^{-4}\omega_{p1}$ (i.e., $\mathrm{Re}[\varepsilon_1(\omega_0)] \approx -100$), and $d_1 = \lambda_0/100$, and a matched uniaxial-DPS slab [see Eqs. (19) and (20)] with $\tau = 0.251$, $\omega_{pa} = 0.992\omega_0$, $\gamma_a = 1.69 \cdot 10^{-4}\omega_{pa}$ (i.e., $\mathrm{Re}[\varepsilon_{2\perp}(\omega_0)] \approx 0.065$ and $\mathrm{Re}[\varepsilon_{2\parallel}(\omega_0)] \approx 3$), and $d_2 = \lambda_0/3$.

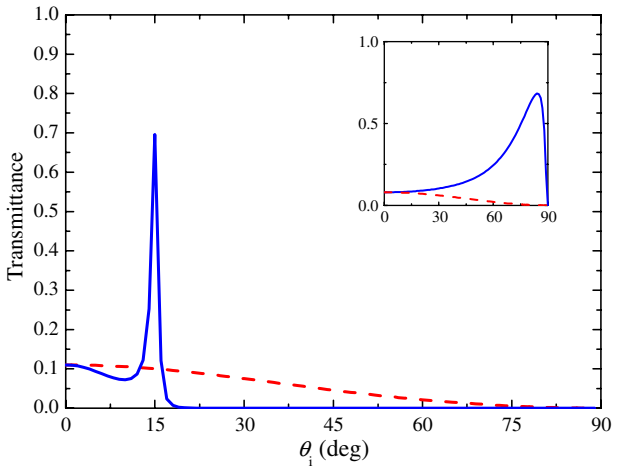

Fig. 8. (Color online) As in Fig. 7, but with an angular response at resonance.

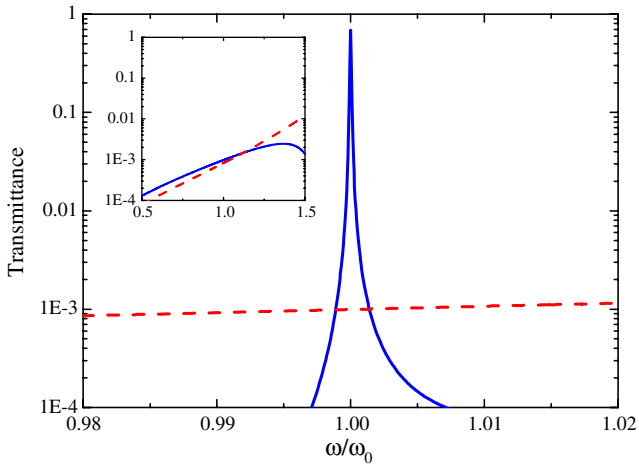

Fig. 9. (Color online) As in Fig. 3, but for an ENG slab [see Eq. (18)] with $\omega_{p1} = 1.58\omega_0$, $\gamma_1 = 3.8 \cdot 10^{-5}\omega_{p1}$ (i.e., $\mathrm{Re}[\varepsilon_1(\omega_0)] \approx -1.5$), and $d_1 = \lambda_0/2$, and a matched uniaxial-DPS slab [see Eqs. (19) and (20)] with $\tau = 0.637$, $\omega_{pa} = 0.962\omega_0$, $\gamma_a = 8.34 \cdot 10^{-6}\omega_{pa}$ (i.e., $\mathrm{Re}[\varepsilon_{2\perp}(\omega_0)] \approx 0.115$ and $\mathrm{Re}[\varepsilon_{2\parallel}(\omega_0)] \approx 1.5$), $\varepsilon_b = 4(1 + 10^{-4}i)$, and $d_2 = \lambda_0/2$. Note the semilog scale and the narrower frequency range considered.

$\mathrm{Re}[\varepsilon_{2\parallel}(\omega_0)] = 3$, i.e., a rather extreme anisotropy. Figures 7 and 8 show the corresponding frequency and angular responses, respectively. By comparison with the previous example (Figs. 3 and 4), qualitatively similar considerations hold, with an increased frequency and angular selectivity [29]. The high-transmittance peak (nearly 70%) turns out to be moderately lower in absolute terms, but considerably higher in terms of enhancement (nearly a factor of 8) with respect to the stand-alone ENG slab.

Finally, in order to include retardation effects, we consider a configuration featuring electrically thicker slabs, namely, $\mathrm{Re}[\varepsilon_1(\omega_0)] = -1.5$, $\mathrm{Re}[\varepsilon_{2\perp}(\omega_0)] = 0.115$, $\mathrm{Re}[\varepsilon_{2\parallel}(\omega_0)] = 1.5$, and $d_1 = d_2 = \lambda_0/2$, for $\theta_{i0} = 30°$ and a reduced level of losses. From the corresponding frequency and angular responses, shown in Figs. 9 and 10, respectively, we observe that the tunneling effect is still possible, although the resonant peaks are much narrower than the previous examples, and the peak transmittance is much more sensitive to the level of losses. This is expected, due to the larger quality factor of

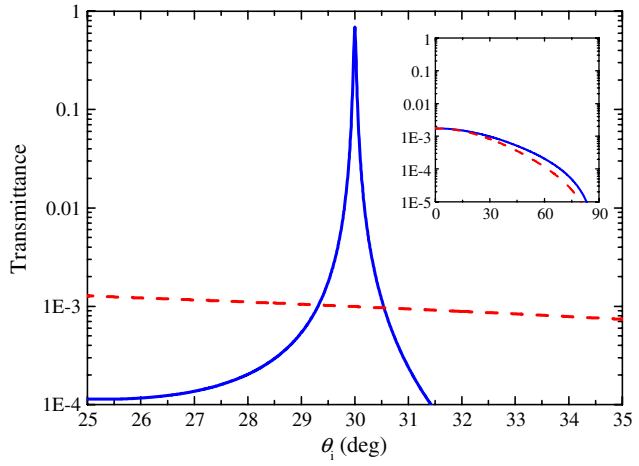

Fig. 10. (Color online) As in Fig. 9, but with an angular response at resonance. Note the semilog scale and the narrower angular range considered.

the resonant tunneling in this example, and it is consistent with similar sensitivity observed in thicker ENG-MNG matched bilayers [3].

5. CONCLUSIONS

In this paper, we have studied an interesting EM tunneling effect that can take place in bilayers featuring a homogeneous, isotropic ENG slab paired with a homogeneous, anisotropic (uniaxial) DPS slab, under appropriate TM-polarized oblique incidence. After a rigorous analytical derivation of the total-transmission conditions (for the ideal lossless case), we have elucidated the underlying physical mechanisms, and we emphasized the strong analogies with the ENG-MNG matched pairs in [3]. Moreover, we have carried out a parametric study aimed at exploring the sensitivity of the phenomenon with respect to frequency, polarization, and incidence direction of the illumination, also taking into account material dispersion and losses.

The possibility of obtaining, for only one polarization, high-transmittance peaks with strong frequency/angular sensitivity (see, e.g., Figs. 7–10) may find application to polarizing frequency/spatial filters or beam splitters. Our results also indicate the possibility of emulating, within narrow frequency/angular ranges, the response of an MNG slab via an arguably simpler to realize uniaxial-DPS slab.

In connection with possible extensions/generalization, we note that the results pertaining to a configuration featuring an MNG slab paired with a uniaxial magnetic DPS slab, under TE-polarized illumination, follow straightforwardly from duality considerations. Finally, it is worth emphasizing that, paralleling the approaches in [30,31], our results may be generalized to tunnel barriers of different nature (e.g., quantum-mechanical).

REFERENCES AND NOTES

1. D. R. Fredkin and A. Ron, "Effective left-handed (negative index) composite material," Appl. Phys. Lett. **81**, 1753–1755 (2002).
2. A. Lakhtakia and C. M. Krowne, "Restricted equivalence of paired epsilon-negative and mu-negative layers to a negative phase-velocity material (alias left-handed material)," Optik **114**, 305–307 (2003).
3. A. Alù and N. Engheta, "Pairing an epsilon-negative slab with a mu-negative slab: resonance, tunneling and transparency," IEEE Trans. Antennas Propag. **51**, 2558–2571 (2003).
4. J. B. Pendry and S. A. Ramakrishna, "Focusing light using negative refraction," J. Phys. **15**, 6345–6364 (2003).
5. H. Jiang, H. Chen, H. Li, Y. Zhang, J. Zi, and S. Zhu, "Properties of one-dimensional photonic crystals containing single-negative materials," Phys. Rev. E **69**, 066607 (2004).
6. L.-G. Wang, H. Chen, and S.-Y. Zhu, "Omnidirectional gap and defect mode of one-dimensional photonic crystals with single-negative materials," Phys. Rev. B **70**, 245102 (2004).
7. L. Zhou, W. Wen, C. T. Chan, and P. Sheng, "Electromagnetic-wave tunneling through negative-permittivity media with high magnetic fields," Phys. Rev. Lett. **94**, 243905 (2005).
8. B. Hou, H. Wen, Y. Leng, and W. Wen, "Electromagnetic wave transmission through subwavelength metallic meshes sandwiched between split rings," Appl. Phys. Lett. **87**, 201114 (2005).
9. G. Guan, H. Jiang, H. Li, Y. Zhang, H. Chen, and S. Zhu, "Tunneling modes of photonic heterostructures consisting of single-negative materials," Appl. Phys. Lett. **88**, 211112 (2006).
10. L. Zhang, Y. Zhang, L. He, H. Li, and H. Chen, "Experimental study of photonic crystals consisting of ε-negative and μ-negative materials," Phys. Rev. E **74**, 056615 (2006).
11. X. Zhou and G. Hu, "Total transmission condition for photon tunnelling in a layered structure with metamaterials," J. Opt. A **9**, 60–65 (2007).
12. Y. Chen, "Defect modes merging in one-dimensional photonic crystals with multiple single-negative material defects," Appl. Phys. Lett. **92**, 011925 (2008).
13. K.-Y. Kim and B. Lee, "Complete tunneling of light through impedance-mismatched barrier layers," Phys. Rev. A **77**, 023822 (2008).
14. Y. Fang and S. He, "Transparent structure consisting of metamaterial layers and matching layers," Phys. Rev. A **78**, 023813 (2008).
15. T. Feng, Y. Li, H. Jiang, Y. Sun, L. He, H. Li, Y. Zhang, Y. Shi, and H. Chen, "Electromagnetic tunneling in a sandwich structure containing single negative media," Phys. Rev. E **79**, 026601 (2009).
16. H. Oraizi and A. Abdolali, "Mathematical formulation for zero reflection from multilayer metamaterial structures and their notable applications," IET Microw. Antennas Propag. **3**, 987–996 (2009).
17. Y. Ding, Y. Li, H. Jiang, and H. Chen, "Electromagnetic tunneling in nonconjugated epsilon-negative and mu-negative metamaterial pair," PIERS Online **6**, 109–112 (2010).
18. C. A. M. Butler, I. R. Hooper, A. P. Hibbins, J. R. Sambles, and P. A. Hobson, "Metamaterial tunnel barrier gives broadband microwave transmission," J. Appl. Phys. **109**, 013104 (2011).
19. G. Castaldi, I. Gallina, V. Galdi, A. Alù, and N. Engheta, "Transformation-optics generalization of tunnelling effects in bi-layers made of paired pseudo-epsilon-negative/mu-negative media," J. Opt. **13**, 024011 (2011).
20. G. Castaldi, I. Gallina, V. Galdi, A. Alù, and N. Engheta, "Electromagnetic tunneling through a single-negative slab paired with a double-positive bilayer," Phys. Rev. B **83**, 081105 (2011).
21. E. Cojocaru, "Electromagnetic tunneling in lossless trilayer stacks containing single-negative metamaterials," Prog. Electromagn. Res. **113**, 227–249 (2011).
22. V. Lomakin and E. Michielssen, "Enhanced transmission through metallic plates perforated by arrays of subwavelength holes and sandwiched between dielectric slabs," Phys. Rev. B **71**, 235117 (2005).
23. It can be verified that the reflection-coefficient denominator is always nonzero.
24. R. Marqués, J. Martel, F. Mesa, and F. Medina, "Left-handed-media simulation and transmission of EM waves in subwavelength split-ring-resonator-loaded metallic waveguides," Phys. Rev. Lett. **89**, 183901 (2002).
25. J. Esteban, C. Camacho-Peñalosa, J. E. Page, T. M. Martín-Guerrero, and E. Márquez-Segura, "Simulation of negative permittivity and negative permeability by means of evanescent waveguide modes—theory and experiment," IEEE Trans. Microw. Theory Tech. **53**, 1506–1514 (2005).
26. P. A. Belov, R. Marqués, S. I. Maslovski, I. S. Nefedov, M. Silveirinha, C. R. Simovski, and S. A. Tretyakov, "Strong spatial dispersion in wire media in the very large wavelength limit," Phys. Rev. B **67**, 113103 (2003).
27. A. Sihvola, *Electromagnetic Mixing Formulas and Applications* (IEE Publishing, 1999).
28. A. Alù, M. G. Silveirinha, A. Salandrino, and N. Engheta, "Epsilon-near-zero metamaterials and electromagnetic sources: tailoring the radiation phase pattern," Phys. Rev. B **75**, 155410 (2007).
29. Note that the transmittance peak in the angular response of the stand-alone ENG slab for near-grazing incidence (see inset in Fig. 8) is attributable to a pseudo-Brewster condition.
30. I. R. Hooper, T. W. Preist, and J. R. Sambles, "Making tunnel barriers (including metals) transparent," Phys. Rev. Lett. **97**, 053902 (2006).
31. L. Jelinek, J. D. Baena, J. Voves, and R. Marques, "Metamaterial-inspired perfect tunneling in semiconductor heterostructures," New J. Phys **13**, 083011 (2010).